Resonance Raman Investigations of *Escherichia coli*-Expressed *Pseudomonas putida* Cytochrome P450 and P420†

Andrew V. Wells, Pusheng Li, and Paul M. Champion*

Department of Physics, Northeastern University, Boston, Massachusetts 02115

Susan A. Martinis‡ and Stephen G. Sligar*

Departments of Biochemistry and Chemistry, University of Illinois at Urbana-Champaign, Urbana, Illinois 61801

Received November 27, 1991; Revised Manuscript Received February 13, 1992

ABSTRACT: High-resolution resonance Raman spectra of the ferric, ferrous, and carbonmonoxy (CO)-bound forms of wild-type *Escherichia coli*-expressed *Pseudomonas putida* cytochrome $P450_{cam}$ and its P420 form are reported. The ferric and ferrous species of P450 and P420 have been studied in both the presence and absence of excess camphor substrate. In ferric, camphor-bound, P450 (m^{os}), the *E. coli*-expressed P450 is found to be spectroscopically indistinguishable from the native material. Although substrate binding to P450 is known to displace water molecules from the heme pocket, altering the coordination and spin state of the heme iron, the presence of camphor substrate in P420 samples is found to have essentially no effect on the Raman spectra of the heme in either the oxidized or reduced state. A detailed study of the Raman and absorption spectra of P450 and P420 reveals that the P420 heme is in equilibrium between a high-spin, five-coordinate (HS,5C) form and low-spin six-coordinate (LS,6C) form in both the ferric and ferrous oxidation states. In the ferric P420 state, H_2O evidently remains as a heme ligand, while alterations of the protein tertiary structure lead to a significant reduction in affinity for Cys(357) thiolate binding to the heme iron. Ferrous P420 also consists of an equilibrium between HS,5C and LS,6C states, with the spectroscopic evidence indicating that H_2O and histidine are the most likely axial ligands. The spectral characteristics of the CO complex of P420 are found to be almost identical to those of a low pH of Mb. Moreover, we find that the 10-ns transient Raman spectrum of the photolyzed P420 CO complex possesses a band at 220 cm^{-1}, which is strong evidence in favor of histidine ligation in the CO-bound state. The equilibrium structure of ferrous P420 does not show this band, indicating that Fe–His bond formation is favored when the iron becomes more acidic upon CO binding. Raman spectra of stationary samples of the CO complex of P450 reveal ν_{Fe-CO} peaks corresponding to both substrate-bound and substrate-free species and demonstrate that substrate dissociation is coupled to CO photolysis. Analysis of the relative band intensities as a function of photolysis indicates that the CO photolysis and rebinding rates are faster than camphor rebinding and that CO binds to the heme faster when camphor is not in the distal pocket.

The heme protein $P450_{cam}$, obtained from *Pseudomonas putida*, has been throughly studied using a variety of physical techniques (Gunsalus et al., 1974; Debrunner et al., 1978; Dawson & Sono, 1987). Because of its ready availability, soluble nature, and extensive characterization, it has become a prototype for the entire family of P450 enzymes. $P450_{cam}$ catalyzes the stereospecific hydroxylation of camphor to form 5-*exo*-hydroxycamphor, in which one atom of dioxygen is inserted into the camphor substrate. The reaction cycle of $P450_{cam}$ (Gunsalus et al., 1974; Debrunner et al., 1978; Dawson & Sono, 1987; Guengerich, 1991) consists of four stable intermediates. The reaction cycle is initiated when the low-spin ferric substrate-free protein (P450 m^o, iron spin $^1/_2$), binds the camphor substrate, and expels a heme-ligated H_2O molecule to form the high-spin state (P450 m^{os}, iron spin $^5/_2$). P450 m^{os} then undergoes a one-electron reduction, with putadaridoxin as the reducing agent, forming the high-spin ferrous state (P450 m^{rs}, iron spin 2). Dioxygen then binds to the heme iron ($m^{rs}_{O_2}$), and a second one-electron reduction takes place, which is followed by rapid product formation via an intermediate that may involve either an iron–oxo π cation radical (Groves et al., 1981) or an oxy radical species (Champion, 1989).

Resonance Raman scattering is a highly sensitive probe of the heme environment and of the iron spin and ligation state, making it ideal for studies of the reaction intermediates of $P450_{cam}$ in aqueous solution. Cytochrome P420 (Gunsalus et al., 1974; Champion et al., 1978; Lipscomb, 1980; Martinis, 1990) is an inactive form of cytochrome P450 that can be formed from all known types of P450 by various methods, such as incubation in acetone (Gunsalus et al., 1974; Champion et al., 1978) or exposure to high temperature or pressure (Hui Bon Hoa et al., 1989; Martinis, 1990). The previous literature on resonance Raman studies of P450 from various species is fairly extensive (Champion et al., 1978; Ozaki et al., 1978; Uno et al., 1985; Bangcharoenpaurpong et al., 1986, 1987; Champion, 1988; Hildebrandt et al., 1989; Anzenbacher et al., 1989; Hu & Kincaid, 1991; Egawa et al., 1991). However, complete resonance Raman studies of the P420 species have not been reported. The chief objectives of this study are to use resonance Raman and absorption spectra to characterize the most common states of P420 and to compare them with the analogous spectra of P450. Particular attention is focused on the ligation state(s) of the P420 form and comparisons are

† This work was supported by the National Institutes of Health Grants AM35090 (P.M.C.), GM31756, GM33775 (S.G.S.), and NSF90-16860 (P.M.C.).

* Authors to whom correspondence should be addressed.

‡ Present address: Department of Biology, Massachusetts Institute of Technology, Cambridge, MA 02139.

0006-2960/92/0431-4384$03.00/0

made to some unusual ligation states of Mb at low pH that have been recently reported (Sage et al., 1991a,b).

Materials and Methods

Using mutant complementation techniques, the structural gene of *P. putida* cytochrome $P450_{cam}$ (Koga et al., 1985) was cloned and inserted into *Escherichia coli* for protein expression as described in Unger et al. (1986), and the $P450_{cam}$ protein was purified. High-purity P420 was prepared by exposure of $P450_{cam}$ to pressures of 2–2.4 kbar at 0.2–25 °C for 1–2 h (Hui Bon Hoa et al., 1989; Martinis, 1990).

P450 and P420 samples were prepared in 0.05 M Tris buffer, pH 7.4, and were approximately 70–150 μM in protein. Substrate-bound samples contained 0.4–1.0 mM camphor and 100 mM KCl. P450 m^o samples were prepared by dialyzing P450 m^{os} against 0.05 M Tris buffer, pH 7.4, for 4 h at ~0 °C, followed by cold centrifugation at ~5500 rpm (3300*g*) with Centricon, Inc., microconcentrators to reconcentrate the samples. Absorption spectra of all samples were taken to ensure sample integrity before and after resonance Raman experiments were performed. Ferrous species were made by chemical reduction using aqueous sodium dithionite in a sealed deoxygenated sample cell. CO-bound samples were prepared by flushing deoxygenated samples with CO gas before addition of sodium dithionite, and data on CO-bound samples were collected in spinning cells to minimize photolysis.

Data were collected using a Spex Triplemate triple monochromator and a Princeton Instruments IRY1024 optical multichannel analyzer (OMA). The continuous illumination laser source for spectra taken at 390, 420, and 440 nm was a Coherent CR-599 tunable CW dye laser with either Exalite 392 or Stilbene III dye (Exciton, Inc.), pumped by a Coherent Innova 100 argon ion laser. The samples excited at 363.8 nm used the UV output directly from the ion laser. The laser power at the sample for the data collected at 390, 420, and 440 nm was typically 10–20 mW after being filtered by a premonochromator. The incident laser power at 363.8 nm was 40–60 mW. The spectra obtained with 10-ns pulsed illumination utilized a Lumonics Hyper-Dye 300 dye laser tuned to 425, 436, or 441 nm, pumped by an Excimer EMG 53 XeCl gas-pulsed laser (Lambda Physik) with a 100-Hz repetition rate. The integration/averaging time for each spectrum was 10–20 min.

All Raman spectra are frequency calibrated using neat fenchone and span the frequency range 200–1000 cm^{-1} and 1050–1700 cm^{-1}, with ~7 cm^{-1} spectral resolution. The sample spectra are flat-field corrected, which entails dividing the sample spectrum by a long-exposure white light spectrum to eliminate the fixed pattern noise due to the diode-to-diode detector response variations.

Results

UV–Visible Absorption Spectra. Figure 1 shows the absorption spectra of the ferric and ferrous species of $P450_{cam}$ and P420. The top panel shows the dramatic 30-nm blue-shift of the Soret band upon introduction of camphor into the heme pocket of P450 m^o. This change corresponds to the expulsion of the H_2O ligand (Atkins & Sligar, 1987; Poulos et al., 1986; Fisher & Sligar, 1987) and the change from a LS,6C[1] to a

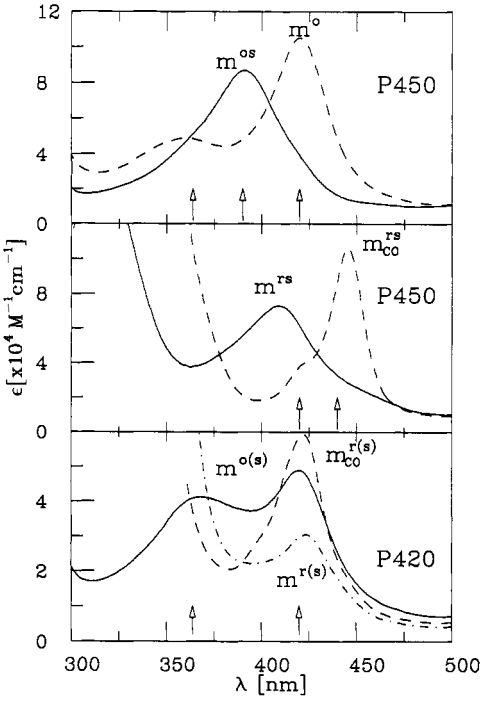

FIGURE 1: Optical absorption spectra for ferric P450 species (top panel), ferrous P450 species (middle panel), and P420 species (bottom panel) investigated in the present work. The m^r spectrum of P450 (not shown) is essentially the same as P450 m^{rs}. The spectra of P420 in the presence of camphor are equivalent to those taken in the absence of camphor. The vertical arrows indicate the excitation wavelengths at which Raman spectra were collected.

HS,5C state (Gunsalus et al., 1974). In contrast, addition of camphor to P420 m^o has no detectable effect on the absorption spectrum (Martinis, 1990), indicating that substrate cannot induce spin and coordination state changes in P420 analogous to those observed in P450. The absorption spectrum of P420 m^o exhibits two Soret bands at ~370 and ~420 nm, and the ratio of these two bands varies depending on how the P450 was converted to P420 (Martinis, 1990). Both P450 m^{rs} and m^r exhibit Soret maxima at 408 nm, in contrast to P420 m^r, which exhibits a Soret peak at 423 nm (Gunsalus et al., 1974; Martinis, 1990). The Soret maxima of P450 m^{rs}_{CO} occur at 447 and 363 nm (Hanson et al., 1976; O'Keeffe et al., 1978; Uno et al., 1985), while the Soret band of P420 m^r_{CO} is found near 423 nm. The arrows in Figure 1 indicate the excitation wavelengths at which resonance Raman spectra were collected.

Comparison of E. coli and P. putida P450 m^{os}. Figure 2 shows Raman spectra of native and *E. coli*-grown $P450_{cam}$ m^{os} at 420 and 390 nm excitation. It is apparent that the protein isolated from *E. coli* exhibits much less fluorescence background, due to the higher degree of purity of the sample. The ν_4 peak is observed to shift from 1372 to 1370 cm^{-1} as the excitation is tuned from 420 to 390 nm, an effect that is due to a superposition of modes (Champion et al., 1978). A depolarized (dp) shoulder on ν_4 at 1384 cm^{-1} can be seen at 390 and 363.8 nm (vide infra), but not at 420-nm excitation. The heme core size marker bands ν_3 and ν_2 appear at 1488 and 1570 cm^{-1}, respectively, indicating a HS,5C state (Spiro, 1983). The depolarized ν_{10} band is identified at 1623 cm^{-1} and is probably accidently degenerate with the vinyl stretching mode $\nu_{C=C}$ (Choi et al., 1982). When P450 m^{os} is excited at 390 nm, the peak of the Soret band, the spectra exhibit very strongly enhanced ν_2 and ν_{10} modes relative to ν_4, in contrast to the much weaker enhancement at 420 nm. A number of depolarized ($\rho \sim 0.3$–0.75) modes also appear in the spectrum at 938, 984, 1007, 1129, 1172, 1225, 1384, 1430, 1525, and

[1] Abbreviations: LS,6C, low spin, six coordinate; HS,5C, high spin, five coordinate; m^o, oxidized, substrate free; m^{os}, oxidized, substrate bound; m^r, reduced, substrate free; m^{rs}, reduced, substrate bound; m^r_{CO}, reduced, CO bound; m^{rs}_{CO}, reduced, substrate and CO bound; m^{rs}*, 10, ns photoproduct of m^{rs}_{CO}; m^{r}* 10-ns photoproduct of m^r_{CO}.

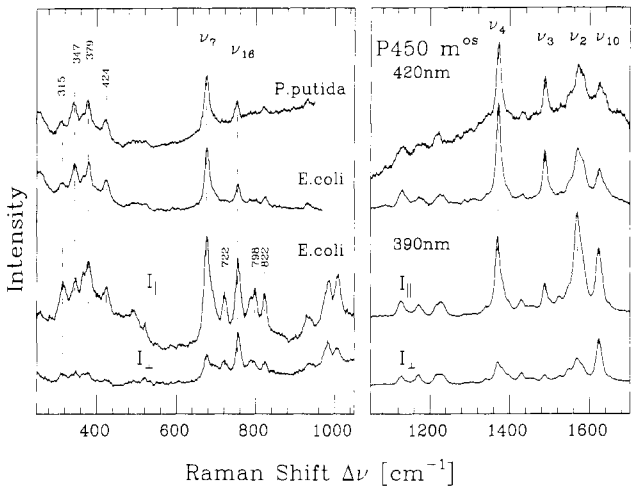

FIGURE 2: Resonance Raman spectra of the ferric camphor-bound (m^{os}) complex of native *P. putida* (top) and the *E. coli*-grown (lower three) cytochrome P450. The excitation wavelength (λ_{ex}) is 420 nm for the two upper spectra. The lower half of the figure shows the parallel and perpendicularly polarized spectra of P450 m^{os} excited with 390-nm illumination. Incident power is 20 mW for *P. putida* and ~30 mW for *E. coli*-grown P450. Integration time is 10 min, and concentrations are 70–100 μM for all samples. Spectra are taken at approximately 4 °C, and the buffer used is 50 mM Tris, pH 7.4, with 1 mM camphor and 100 mM KCl. These spectra have been flat-field corrected as described in the text. For the upper two samples, the intensities of the low-frequency spectra are multiplied by 2 relative to the corresponding high-frequency spectra. For the data at 390-nm excitation, the low-frequency spectra are multiplied by 5 relative to high frequencies.

Table I: Observed Low-Frequency Modes[a]

sample	ν_8	*b*	*b*	ν_7	ν_{16}
P450 m^{os}	347	379	424	678	755
P420 m^{os}	347	377	418	678	752
P450 m^{o}	347	379	424	678	753
P420 m^{o}	347	377	418	678	752
P450 m^{rs}	363	377	415	674	747
P420 m^{rs}	345	380	418	675	749
P450 m^{r}	345	378	420	674	747
P420 m^{r}	345	380	418	675	748
P450 m^{rs}_{CO}	352	379	423	676	749
P420 m^{r}_{CO}	348	379	418	677	754

[a] All units are cm^{-1}; λ_{ex} ~420 nm except for P450 m^{rs}_{CO}, which is 440 nm. [b] The second two columns of data are unassigned modes shown in Figures 2, 3, 4, 6, and 7.

1547 cm^{-1}. The set of peaks near 1000 cm^{-1} are relatively strongly enhanced with 390-nm excitation.

At low frequencies, the assigned heme skeletal modes in P450 m^{os} are ν_7 (677 cm^{-1}), ν_{16} (dp, 756 cm^{-1}), and ν_8 (347 cm^{-1}). Other low-frequency modes appearing at 315, 379, 424, 691, 722, 788, 798, and 822 cm^{-1} are more difficult to assign because they do not correlate well with low-frequency modes found in model compounds for which complete normal mode anlayses are available (Abe et al., 1978; Choi & Spiro, 1983; Li et al., 1989, 1990a,b). The polarization characteristics of the Raman modes of P450 m^{os} at 390 nm can be observed by comparing the spectrum of parallel polarized scattering ($I_\parallel$) with that of perpendicular polarized scattering ($I_\perp$) in Figure 2.

Ferric P450 and P420 Excited at 420 nm. Figure 3 compares the Soret enhanced Raman spectra of P450 and P420 in the presence and absence of 1 mM camphor. The frequencies of the Raman lines of interest are given in Tables I and II. The excitation wavelength (420 nm) is at or near the Soret peak for each species except P450 m^{os}. In all four samples, the oxidation marker band ν_4 is in the 1372–1374-

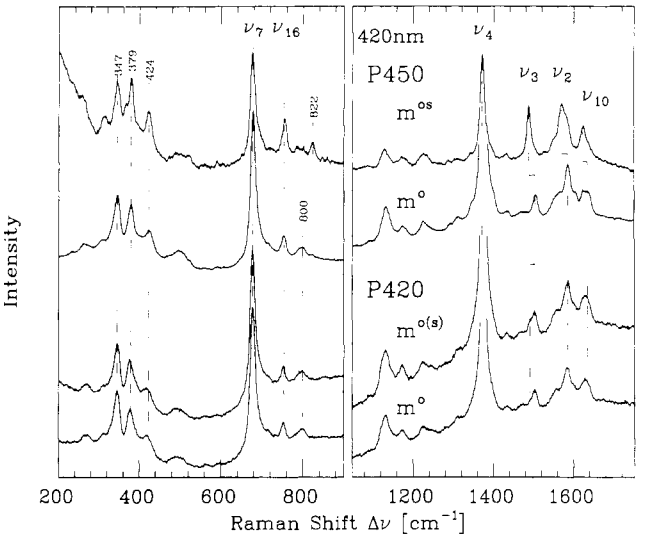

FIGURE 3: Resonance Raman spectra of the ferric species of *E. coli*-grown P450 and P420 at λ_{ex} = 420 nm. Spectra of P450 and P420 samples in the presence [$m^{o(s)}$] and absence (m^o) of 1 mM camphor are shown. Incident powers are 35, 20, 15, and 28 mW, respectively, for P450 m^{os}, P450 m^o, P420 $m^{o(s)}$, and P420 m^o. All other conditions are the same as given in the legend to Figure 2. The low-frequency spectrum of the P450 m^{os} is multiplied by a factor of 3, and the low-frequency spectra of the P420 $m^{o(s)}$ samples are multiplied by a factor of 1.3, relative to their corresponding high-frequency spectra. The intensity scale for the P450 m^o sample is the same for high and low frequencies.

Table II: Observed Heme Core Marker Bands[a]

sample	ν_4	ν_3	ν_2	ν_{10}[b]	assignment
P450 m^{os}	1368	1488	1570	1623[c]	HS,5C
	1372		1582	1637[c]	LS,6C
P420 m^{os}	1374	1503	1588	1629	LS,6C
		1491	1572		HS,5C
P450 m^{o}	1373	1503	1584	1635	LS,6C
P420 m^{o}	1374	1503	1588	1629	LS,6C
		1491	1572		HS,5C
P450 m^{rs}	1345	1466	1564	1601	HS,5C
P420 m^{rs}	1361	1493	1583	1620[c]	LS,6C
		1470	1560	1603	HS,5C
P450 m^{r}	1345	1468	1563	1601	HS,5C
P420 m^{r}	1361	1493	1583	1620[c]	LS,6C
		1470	1560	1603	HS,5C
P450 m^{rs}_{CO}	1371	1497	1588		LS,6C
P420 m^{r}_{CO}	1372	1498	1583	1626	LS,6C

[a] All units are cm^{-1}, λ_{ex} = 420 nm except for P450 m^{rs}_{CO}, which is 440 nm. [b] Assigned using depolarized component of RR spectrum. [c] $\rho \sim 0.5$ indicates that the ν_{10} mode is accidently degenerate with $\nu_{C=C}$.

cm^{-1} range, indicating the ferric state.

Upon binding camphor to P450 m^o, the ν_3 and ν_2 modes undergo significant spectroscopic changes, as can be observed in Figure 3. The frequencies of these modes are sensitive to porphyrin core size and thus to the iron spin and coordination state (Spaulding et al., 1975; Spiro, 1983). The ν_3 mode in P450 m^o is at 1503 cm^{-1}, consistent with a LS,6C state in which the thiolate sulfur of Cys(357) is coordinated to the proximal side of the heme iron and a water molecule is coordinated to the distal side (Atkins & Sligar, 1987; Poulos et al., 1986). In the camphor-bound complex, the ν_{10} and the ν_2 modes downshift by 12 and 14 cm^{-1}, respectively, which, along with the downshift of the ν_3 mode to 1488 cm^{-1}, is consistent with a HS,5C state in which the iron-coordinated water molecule has been expelled.

In Figure 3 it can be seen that the spectra of P420 solutions with camphor absent (labeled m^o) or present [labeled $m^{o(s)}$] are nearly indistinguishable. The lack of significant change

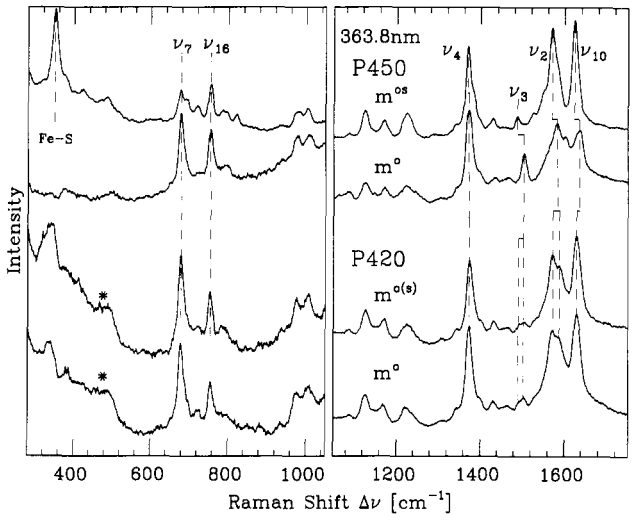

FIGURE 4: Resonance Raman spectra of the ferric species of cytochrome P450 and P420 at λ_{ex} = 363.8 nm. Incident powers are 55–60 mW, defocused. All other conditions are the same as those of Figure 2. The askerisks indicate quartz scattering from the sample cell. The low-frequency spectra of P450 m^{os}, P450 m^{o}, P420 m^{o}, and P420 m^{os} are multiplied by factors of 2.3, 5, 4, and 4, respectively, relative to the corresponding high-frequency spectra. Note the very large Fe–S mode at 350 cm^{-1} in P450 m^{os}, which is absent in the P450 m^{o} spectrum.

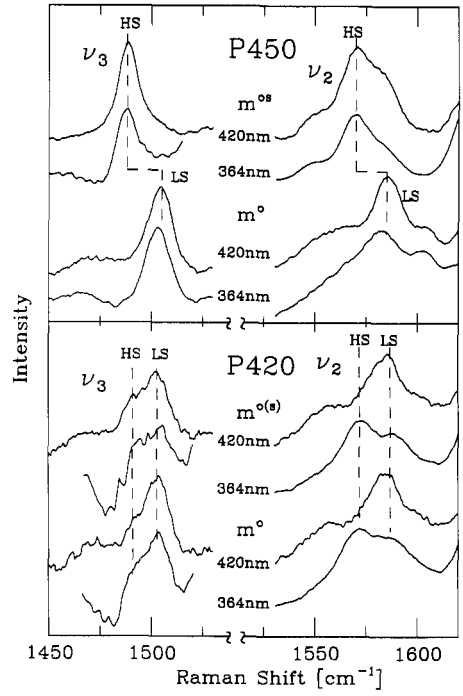

FIGURE 5: Evidence for mixed ligation state in P420 m^{o}. The upper panel shows the ν_3 and ν_2 regions for P450 m^{os} and P450 m^{o} at λ_{ex} = 420 and 363.8 nm. The lower box shows expanded plots of the ν_3 and ν_2 regions of P420 $m^{o(s)}$ and P420 m^{o} at λ_{ex} = 420 and 363.8 nm. The iron spin and coordination states of the samples are determined from the positions of the heme core size marker bands (ν_3 and ν_2) as indicated. The vertical scales of the P420 spectra in the ν_3 region are expanded relative to the respective curves in the ν_2 region. Note that as the excitation wavelength is shifted into resonance with the ~370-nm absorption band of P420 m^{o} (see Figure 1), the HS,5C marker bands are enhanced, indicating that this absorption band corresponds to the HS,5C population of P420. The resonance enhancement pattern of the ν_3 mode is complicated by non-Condon effects (Morikis et al., 1991).

in the important ν_3 and ν_2 region indicates that the spin and coordination state of the iron is insensitive to the presence of camphor. In addition, the double-peaked Soret absorption spectrum of P420 m^{o} (Figure 1) is unaltered by the addition of camphor (Martinis, 1990), again suggesting that the heme environment of ferric P420 is unaffected by the presence of camphor.

It is clear from Figure 3 that at 420-nm excitation, the two ferric P420 spectra (with and without camphor) strongly resemble the P450 m^{o} spectrum except in the ν_3 region, where ferric P420 exhibits two polarized modes at 1491 and 1503 cm^{-1}. The former mode, associated with a HS,5C species, is absent from the P450 m^{o} spectrum. In addition, we note that the absorption spectra of P450 m^{o} and P420 m^{o} differ markedly (see Figure 1). The P420 m^{o} species possesses at least two Soret band components at 420 and ~370 nm, while the latter band[2] is absent from the spectra of P450 m^{o}.

Ferric P450 and P420 Excited at 363.8 nm. Figure 4 shows the same species as Figure 3, but using 363.8-nm excitation, which is out of resonance with the Soret bands of P450 m^{o} and P420 at ~420 nm, but still in resonance with the 390 nm Soret band of P450 m^{os} and the ~370-nm band of P420 m^{o}. Figure 4 again shows the dramatic effect of camphor binding on ferric P450 as well as the lack of any effect in ferric P420. The spin-state related shifts of ν_3 and ν_2 seen in the P450 spectra of Figure 3 are also present in Figure 4. In addition, a small mode at 1604 cm^{-1} in P450 m^{o} disappears on camphor binding. In P450 m^{os}, the ν_4 mode appears to shift from 1372 to 1368 cm^{-1} when the excitation wavelength is tuned from 420 to 363.8 nm. This effect, which has been observed previously, is due to mode superposition (Champion et al., 1978) and is not observed in P450 m^{o} or in ferric P420.

The other high-frequency skeletal modes of ferric P420 resemble a mixture of the P450 m^{os} (HS) and P450 m^{o} (LS) spectra. As in Figure 3, P420 exhibits two modes at 1491 and 1503 cm^{-1}, corresponding to HS,5C and LS,6C iron ligation states. The ν_2 mode is often more difficult to assign because the depolarized mode ν_{11} and the inversely polarized ν_{19} mode frequently underlie ν_2 (Choi et al., 1982; Morikis, 1990), and it is usually found that ρ = ~0.2–0.3 for ν_2. P420 m^{o} exhibits two modes in the ν_2 region with ρ in this range, at 1572 (HS,5C) and 1588 cm^{-1} (LS,6C). The $\nu_{10}/\nu_{C=C}$ region of ferric P420 resembles P450 m^{os} except that the depolarized ν_{10} mode is shifted to 1629 from 1623 cm^{-1}. In P450 m^{o} the ν_{10} mode is shifted to 1635 cm^{-1}.

The low-frequency mode patterns of Figure 4 follow many of the same trends as Figure 3, with the additional feature of the strongly enhanced Fe–S stretching mode at 351 cm^{-1} in P450 m^{os} (Champion et al., 1982). This mode is completely absent from the P450 m^{o} spectrum, indicating that the charge transfer transitions that enhance the Fe–S mode (Bangcharoenpaurpong et al, 1987; Champion, 1989) are absent when the iron is low spin. A broad, weak mode at ~340 cm^{-1} also appears in the ferric P420 spectra and might be associated with an altered Fe–S geometry of a minority high-spin fraction (see Discussion). Several additional, partially depolarized modes can be observed in P450 m^{os} in the 650–850-cm^{-1} range using excitations at 363.8 and 390 nm (see Figure 2), but not at 420

[2] Note that the position of the blue-shifted component of the P450 m^{o} absorption spectrum at 358 nm is consistent with a N-band assignment, based on the spectrum of ferricytochrome *c* (N-band at 355 nm). The resonance Raman excitation profiles of P450 m^{o} (Bangcharoenpaurpong et al., 1987) are also consistent with the N-band assignment, since increased enhancements of the Raman intensities are not observed with excitation in this region. In contrast, the Raman excitation profiles of the CO complex of P450 (Morikis et al., 1991) show a significant enhancement at 364-nm excitation, confirming a hyperporphyrin assignment (Hanson et al., 1976) for the split Soret absorption band of this complex.

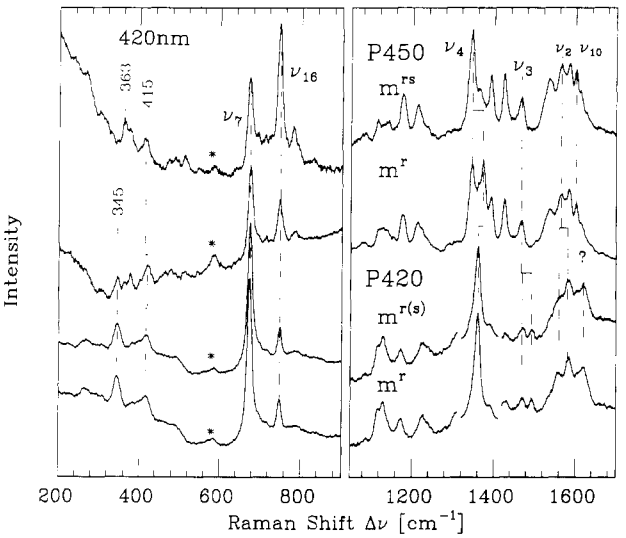

FIGURE 6: Resonance Raman spectra of the ferrous species of *E. coli*-grown P450 and P420 at λ_{ex} = 420 nm. Shown are the m^{rs} and m^r forms of P450, as well as the P420 complex in the presence [$m^{r(s)}$] and absence (m^r) of 1 mM camphor. The low-frequency spectra of P450 m^{rs} and m^r are multiplied by 2.3 and 2.8, respectively, relative to the corresponding high-frequency spectra. The low-frequency spectra of P420 $m^{r(s)}$ and m^r are divided by factors of 1.2 and 1.2, respectively, relative to the high-frequency spectra. The ν_4 regions of the P420 samples are divided by factors of 3 relative to the rest of the high-frequency spectra. Incident powers are 29, 26, 34, and 25 mW, respectively, for P450 m^{rs}, P450 m^r, P420 $m^{r(s)}$, and P420 m^r. All other conditions are the same as those of Figure 2. The high- and low-frequency P450 m^r spectra shown have been modified to eliminate P420 m^r impurity (about 10%) by subtracting the corresponding P420 m^r spectra so that the strong ν_4 peak due to P420 m^r at 1361 cm^{-1} is eliminated.

nm. Also, there is a distinct difference in the intensity ratio of ν_7 to ν_{16} in P450 m^{os} relative to the other three samples. This ratio is slightly less than 1 in P450 m^{os}, and in the other three samples it is ~2.

The ν_3 and ν_2 Modes of Ferric P450 and P420. Figure 5 shows expanded plots of the ν_3 and ν_2 regions of the ferric P450 and P420 Raman spectra. The upper panel displays the distinct spin state change observed when camphor binds to P450 m^o, showing the ν_3 shift from 1503 (LS,6C) to 1488 cm^{-1} (HS,5C) and the ν_2 shift from 1584 (LS,6C) to 1570 cm^{-1} (HS,5C). In contrast, the relative intensities of the LS,6C and HS,5C modes in ferric P420 indicate the presence of both spin states in the sample. In the ν_2 region, the 1572-cm^{-1} mode (HS,5C) is more strongly enhanced at 363.8-nm excitation, while the 1588-cm^{-1} mode (LS,6C) is more strongly enhanced at 420 nm. A similar effect is seen for the ν_3 modes, but it is less pronounced.[3] Since the 370-nm absorption band of P420 m^o enhances the HS,5C modes more strongly, we suggest that this absorption band is associated with a HS,5C state. Similarly, the 420-nm absorption band enhances the low-spin Raman bands and is associated with the LS,6C state. Finally, we note that a careful examination of the P420 spectra in Figure 5 reveals a barely detectable camphor-induced increase in the relative intensities of the HS,5C modes.

[3] The ν_3 mode Raman excitation profiles (REP) are complicated in P450 m^{os} (Bangcharoenpaurpong et al., 1987) and other heme proteins (Morikis et al., 1991) by relatively strong non-Condon coupling effects. This leads to double-peaked REP's, with maxima to the red and blue of the absorption band (Morikis et al., 1991). The complicated REP behavior reduces the selective enhancement of the HS,5C and LS,6C ν_3 modes as the excitation wavelength is varied between 420 and 364 nm in Figure 5.

Ferrous P450 and P420 Excited at 420 nm. Figure 6 shows the fully reduced forms of P450 and P420 excited at 420 nm in the presence and absence of camphor. The ν_4 bands of P450 m^{rs} and m^r appear at 1345 cm^{-1}, indicating the ferrous state, but are significantly shifted to lower frequency due to the electron donation of the thiolate sulfur ligand (Champion et al., 1978; Ozaki et al., 1978; Anzenbacher et al., 1989). This electron-rich ligand causes electron density to shift from the iron to the antibonding orbitals of the heme, weakening the heme bonds. The heme core size markers ν_3 and ν_2 appear at 1468 and 1563–1564 cm^{-1}, indicating the ferrous HS,5C state, and these modes are also anomalously downshifted due to the thiolate sulfur electron donation. The depolarized ν_{10} band of the heme has been identified at 1601 cm^{-1} by analysis of its polarization properties.

Overall, the high-frequency spectra of P450 m^{rs} and m^r are very similar except for the important difference that P450 m^r exhibits a additional strong ν_4 mode at 1372 cm^{-1}. Both P450 m^{rs} and m^r exhibit additional modes in the important 1300–1700-cm^{-1} range. This set of bands includes both depolarized and partially depolarized (pp) modes, which occur at 1392 (dp), 1424 (dp), 1536 (pp), 1586 (pp), and 1612 cm^{-1} (pp). The ν_4 mode observed at 1372 cm^{-1} in the cw Raman spectrum of P450 m^r is not detected in the cw spectra of P450 m^{rs} or P420 m^r. However, we find that under conditions of pulsed laser excitation at 390 nm, P450 m^{rs} also exhibits a 1372-cm^{-1} mode, with a flux-dependent intensity. This, along with changes in the low-frequency region, suggests that photooxidation might be taking place in the P450 system and is enhanced in the absence of substrate. The redox potentials of camphor-free and camphor-bound P450 (Sligar & Gunsalus, 1976) also suggest this possibility. Further studies will be needed to substantiate the hypothesis of photooxidation. We also note that, if a ν_4 mode appears at 1372 cm^{-1} in a ferrous oxidation state, it is indicative of tetracoordinate heme iron (Andersson et al., 1989; Sage et al., 1991a). The possibility of photolysis of the sulfur ligand cannot be ruled out, but enhancement of such a species using 420-nm excitation appears unlikely (Sage et al., 1991a).

At low frequencies, P450 m^{rs} and m^r exhibit a significant difference in the intensity ratio of the skeletal modes ν_7 and ν_{16} and the relative intensities of the 345 and 363 cm^{-1} modes. This may also be due, at least partially, to the presence of photooxidized material in the spectrum of m^r. Assignment of the low-frequency heme modes is complicated by the lack of strong correlations between the observed ferrous P450 modes and those of model compounds upon which the normal mode calculations are based (Abe et al., 1978; Choi & Spiro, 1983; Li et al., 1989, 1990a,b).

As shown in Figure 6, the Raman spectra of ferrous P420 are quite different from those of P450 m^{rs} and m^r and are completely unaffected by the presence of camphor, demonstrating that camphor does not significantly perturb the heme site. The ν_4 mode of ferrous P420 is upshifted to 1361 cm^{-1} relative to that of P450 m^{rs} and m^r, indicating the absence of thiolate electron donation to the heme iron in P420. Ferrous P420 exhibits two polarized bands in the ν_3 region, at 1470 and 1493 cm^{-1}. Two potential ν_2 bands are also present, at 1559 and 1583 cm^{-1}, and have $\rho \simeq 0.2$–0.3, as is commonly observed for this mode (Choi et al., 1982; Morikis, 1990). The lower frequency bands of the ν_3 and ν_2 regions (1470 and 1559 cm^{-1}) are assigned as HS,5C modes and the higher frequency bands (1493 and 1583 cm^{-1}) as LS,6C modes, as reported in Table II. The depolarized heme mode ν_{10} has not been definitely identified in ferrous P420, although there is a partially

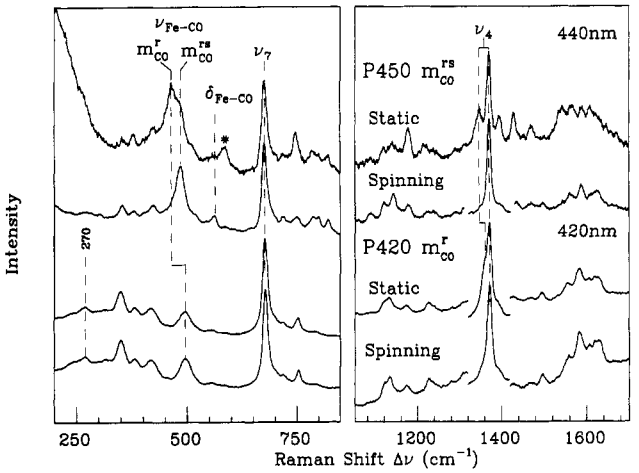

FIGURE 7: Resonance Raman spectra of the CO adducts of P450 and P420, with camphor present, at λ_{ex} = 440 nm for P450 and λ_{ex} = 420 nm for P420. Spectra of both static and spinning samples are shown. The low-frequency spectrum of P450 m^{rs}_{CO} in the static cell is multiplied by 1.5 relative to the high-frequency spectrum, while the spinning sample has the low-frequency spectrum and ν_4 divided by 1.3 and 2 relative to the high-frequency spectrum. The low-frequency spectra and the ν_4 modes of the static and spinning P420 samples are divided by (2, 1.5) and (2.4, 2.6), respectively, relative to the high-frequency spectra. All other conditions are the same as those of Figure 2. Note that in the static P450 spectrum two Fe–CO modes appear, at 465 and 484 cm^{-1}, corresponding to the camphor-free and camphor-bound states, respectively. The ν_4 mode clearly shows partial photolysis of the CO ligand in the static P450 sample, where two peaks can be seen at 1346 and 1371 cm^{-1}, corresponding to the m^{rs} and m^{rs}_{CO} states, respectively. The static spectrum of P450 has contributions from m^{rs}_{CO}, m^r_{CO}, m^{rs}, and m^r. The mode at ~580 cm^{-1} is due to dithionite.

depolarized mode detected at 1620 cm^{-1}. The strongly enhanced high-frequency depolarized modes at 1392 (ν_{29}) and 1424 cm^{-1} [δ_s (=CH_2)] in P450 m^{rs} and m^r are much more weakly enhanced in ferrous P420 relative to ν_4. The low-frequency spectrum of ferrous P420 differs sharply from either P450 m^{rs} or m^r. For example, the ν_7 mode is much more strongly enhanced than the ν_{16} mode in P420 m^r, compared to P450 m^{rs} and m^r. The modes of ferrous P420 at 345 and 415 cm^{-1} are also found to be relatively strongly enhanced at 420-nm excitation.

Ferrous CO Complex of P450 and P420. Figure 7 shows resonance Raman spectra of the CO adducts of P450 and P420, collected using spinning and stationary sample cells. The spinning cell spectrum of P450 m^{rs}_{CO} exhibits a single ν_4 band at 1371 cm^{-1}, indicating no detectable CO photolysis. The ν_{Fe-CO} mode in the spinning sample is observed at 484 cm^{-1}, and the δ_{Fe-CO} mode is at 560 cm^{-1}, which is in close agreement with the measurements of Uno et al. (1985) for the substrate-bound material. The static cell spectrum shows an additional ν_4 band at 1346 cm^{-1} that is associated with P450 m^{rs} and indicates partial CO photolysis and an intact thiolate iron bond. Since P450 m^{rs} and P450 m^{rs}_{CO} have Soret maxima at 408 and 447 nm, respectively, the CO adduct is in much stronger resonance with the 440-nm excitation, as indicated by the intense ν_4 mode of the CO-bound species. The static cell spectrum also exhibits many other bands in the high- and low-frequency regions characteristic of P450 m^{rs}. The most striking feature of the static cell spectrum, however, is the appearance of a doublet in the ν_{Fe-CO} region, with bands at 465 and 484 cm^{-1}. The band at 465 cm^{-1} corresponds to ν_{Fe-CO} for P450 m^r_{CO}, the substrate-free CO adduct of P450 (Uno et al., 1985). This indicates that substrate dissociation is coupled to CO photolysis and that the CO rebinds prior to the substrate so that a significant population of m^r_{CO} is created. The corresponding doublet in the δ_{Fe-CO} mode cannot be resolved since

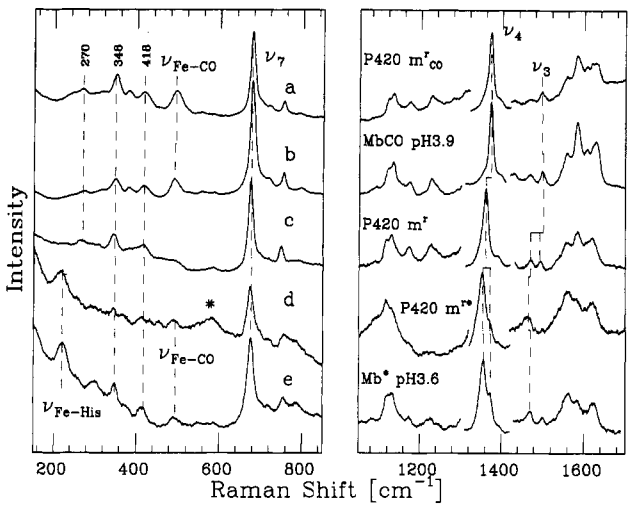

FIGURE 8: Resonance Raman spectra of P420 m^r_{CO} at pH 7.0 (a) and MbCO at pH 3.9 (b), both in spinning cells and excited with continuous illumination at 420 nm. The bottom three spectra are P420 m^r excited cw at 420 nm (c), the 10-ns transient photoproduct of P420 m^r_{CO} (m^{r*}) excited with 10-ns pulsed illumination at 436 nm in a spinning cell (d), and the 10-ns transient photoproduct of MbCO (Mb*), pH 3.6, excited with a 10-ns pulsed laser at 441 nm, in a spinning cell (e). The asterisk indicates a peak near 580 cm^{-1} due to the sodium dithionite reducing agent. The incident pulsed laser (100 Hz) had an average power of 9 mW for the P420 sample and 5 mW for the Mb sample. The intensities of the low-frequency spectra and ν_4 are rescaled (divided) relative to the high-frequency spectra by 1.2, 3 (a); 2.9, 5 (b); 2.4, 3 (c); 1.6, 2 (d); 1, 2 (e), respectively.

the substrate-bound and substrate-free frequencies are 558 and 556 cm^{-1}, respectively (Uno et al., 1985). The mode observed near 580 cm^{-1} is due to Raman scattering of dithionite.

In contrast, the CO complex of P420 shows only a single ν_{Fe-CO} mode, even when photolyzed in a static cell. The increased intensity of the photolyzed ν_4 band in the static spectrum of P420 $m^{r(s)}_{CO}$ is a reflection of the fact that ferrous P420 has its Soret maximum very close to that of the CO adduct (423 and 422 nm, respectively). The only effect of camphor on P420 is to reduce the level of photolysis in the static cell experiment. The ν_{Fe-CO} mode of P420 m^r_{CO} is found at 494 cm^{-1}, upshifted by ~30 cm^{-1} from the ν_{Fe-CO} mode of P450 m^r_{CO}.

Ferrous CO Complex of P420 and the 10-ns Photoproduct. The upper two spectra in Figure 8 show the striking similarity between the 420-nm (cw) excited Raman spectra of P420 m^r_{CO} (a) and MbCO at pH 3.9 (b). In the heme core size marker region, ν_4 is found at 1372 cm^{-1} in P420 m^r_{CO} and at 1374 cm^{-1} in low pH MbCO. The ν_3 bands are at 1498 and 1501 cm^{-1}, respectively. Polarization analysis can be used to assign the peaks near 1470 cm^{-1} in panels a and b to a B_{2g} mode ν_{28} (Anzenbacher et al., 1989). The 1550–1650-cm^{-1} region, containing ν_2, ν_{10}, and $\nu_{C=C}$, shows nearly the same mode pattern in both samples. At low frequencies, the chief difference is that the ν_{Fe-CO} mode lies at 494 cm^{-1} for P420 m^r_{CO} and at 491 cm^{-1} for low pH MbCO.

The lower three spectra in Figure 8 show the 10-ns transient Raman spectra of P420 m^r_{CO} (d) and low pH MbCO (e) obtained using a pulsed laser. The equilibrium spectrum of P420 m^r obtained with a cw laser is also shown for reference (c). The 10-ns transient Raman spectra of P420 m^r_{CO} (m^{r*}) and low pH MbCO (Mb*) appear to be quite similar. Both exhibit doublets in the ν_4 region, but the ν_4 corresponding to the photolyzed state is at 1357 cm^{-1} in low pH Mb* and at 1354 cm^{-1} in P420 m^{r*}. The ν_3 band appears at about 1470 cm^{-1} in both samples, indicating a HS,5C state. Both samples also exhibit similar mode patterns in the 1550–1650-cm^{-1}

range. Superimposed spectra, due to the unphotolyzed material, account for the additional ν_3 peaks near 1500 cm^{-1}.

In the low-frequency region, a distinct band at 218 cm^{-1} appears in both transient spectra. In low pH Mb, this band has been assigned to the ν_{FeHis} mode (Sage et al., 1991b), and, on the basis of the spectral similarities depicted in Figure 8, we propose the same assignment for P420 m^{r*}. Excitation for spectrum d is at 436 nm, while excitation for spectrum e is at 440 nm. The intensity of the 218-cm^{-1} mode is found to decrease in Raman spectra of m^{r*} taken at 425 nm, suggesting that the Soret maximum of the transient species is similar to that of deoxy-Mb (λ_{max} = 435 nm). Finally, we note that the ν_4 mode is found at 1354 cm^{-1} in the transient P420 m^{r*} spectrum and at 1361 cm^{-1} in the equilibrium P420 m^r spectrum. More importantly, the equilibrium spectrum of P420 m^r does not exhibit the 218-cm^{-1} mode found in the 10-ns transient spectrum.

Discussion

We have observed that *E. coli*-expressed $P450_{cam}$ is spectroscopically indistinguishable from the native material. Previous Raman investigations (Champion et al., 1978) of P450 m^{os} using native material revealed a small, excitation wavelength dependent, frequency shift of the ν_4 mode. This same behavior is observed in the *E. coli*-expressed samples and is attributed to a LS,6C subpopulation (<10%) of substrate-free cytochrome (m^o) that has a strongly enhanced ν_4 mode at 1372 cm^{-1} when excited near the 420-nm absorption maximum (see Figure 1). Similarly, the Raman spectrum of the predominant HS,5C, substrate-bound population is enhanced near its absorption maximum at 390 nm and displays a ν_4 band at 1368 cm^{-1}.

The significant spin and coordination state changes that occur in P450 m^o upon camphor binding are not observed in oxidized, reduced, or CO-bound P420. This implies that if camphor binds to P420, it does not displace the H_2O heme ligand or alter the heme environment or CO binding geometry. This is consistent with the findings of Martinis (1990), which report that the introduction of camphor has no effect on the optical or EPR spectra of either ferric or ferrous P420. However, we do find that the presence of camphor leads to a decrease in the photolyzed fraction of the P420 CO complex. This suggests that CO escape from the heme pocket of P420 might somehow be hindered by camphor binding.

Ligation State of Ferric P420. Ferric P420 is observed to possess two ν_3 modes at 1491 and 1503 cm^{-1} and two ν_2 modes at 1572 and 1588 cm^{-1}. The lower frequency modes in each pair are associated with the HS,5C state and the higher frequency modes with the LS,6C state. Furthermore, as shown in Figure 5, the HS,5C and LS,6C modes are probably associated with the two Soret absorption bands found in P420 at ~370 and 420 nm, respectively. This suggests that ferric P420 consists of an equilibrium between at least two spin/coordination states. However, the axial heme ligand in the HS,5C state of ferric P420 must differ from the Cys(357) ligand of P450 m^{os}, since the HS Soret band of ferric P420 (~370 nm) is blue-shifted by at least 20 nm relative to that of P450 m^{os} (390 nm) and no clear Fe–S mode at 351 cm^{-1} is observed. In contrast, the LS,6C Soret band of ferric P420 is at approximately the same position as that of P450 m^o (~420 nm). This, along with the very similar Raman spectra, suggests that the LS,6C component of ferric P420 has the same axial heme ligands as P450 m^o [Cys(357) and H_2O]. A simple chemical equilibrium can then be used to describe the heme ligation in the oxidized P420 state.

$$S^-_{Cys}\text{–}Fe^{3+} + OH_2 \underset{}{\overset{K_1}{\rightleftharpoons}} S^-_{Cys}\text{–}Fe^{3+}\text{–}OH_2 \overset{K_2}{\rightleftharpoons} S^-_{Cys} + Fe^{3+}\text{–}OH_2 \quad (1)$$

HS,5C — LS,6C — HS,5C

λ_{max} ~ 390 nm — λ_{max} ~ 420 nm — λ_{max} ~ 370 nm

This simple model is consistent with the idea that the equilibrium constants (K_1 and K_2) for ligation of amino acids or water to the heme are a strong function of tertiary protein structure (Sage et al., 1991a,b). The absorption and Raman data suggest that the ferric P420 tertiary structure destabilizes the Cys(357)–Fe bond, and possibly the H_2O ligation. When the sulfur ligand dissociates, the remaining HS,5C state should resemble metMb below pH 4, a species that is high-spin and pentacoordinate, with H_2O as the most likely[4] fifth ligand (Sage et al., 1991a). This is in fact the case, since low pH metMb possesses an broad absorption band at ~370 nm (Sage et al., 1991a). Moreover, the Raman spectra of ferric P420 (Figure 4) and low pH metMb excited at 363.8 nm [Figure 3 of Sage et al. (1991a)] show strong similarities. These observations suggest that tertiary conformational changes take place in P420 that destabilize the ligation of Cys(357) to the heme and shift the equilibrium toward a 5C state, with H_2O (or some other unknown coordinating species) as the fifth ligand.

In addition to the 5C water-ligated state, the observation of a broad, relatively weak, mode at ~340 cm^{-1} in the P420 Raman spectra of Figure 4 suggests the presence of a distribution of protein structures that maintain a Fe–S bond but have geometries different from P450. These states would correspond to a HS fraction of ferric P420 where protein tertiary changes alter the Fe–S geometry and lead to H_2O dissociation (see the left side of eq 1). The possible existence of such states cannot be excluded by the P420 absorption spectrum of Figure 1, since the Soret band would be expected near ~390 nm and could be hidden within the broad Soret band line shapes.

Ligation State of Ferrous P420. Spectroscopic evidence suggests that the ligation state of P420 m^r is quite different from that of the thiolate-ligated ferrous P450. For example, the absorption and Raman spectra of P420 m^r differ sharply from those of P450 m^{rs} and m^r. In particular, the position of the heme skeletal mode ν_4 downshifts from 1361 cm^{-1} in P420 m^r to 1345 cm^{-1} in P450 m^{rs} and m^r. The down-shifted P450 m^{rs} ν_4 position is caused by the presence of the strongly electron-donating thiolate ligand (Ozaki et al., 1978; Champion et al., 1978; Chottard et al., 1984; Anzenbacher et al., 1989). The ν_4 position of P420 m^r is more characteristic of weaker ligands such as methionine, histidine, or water (e.g., ferrocytochrome *c*, ν_4 = 1361 cm^{-1}; deoxyMb, ν_4 = 1357 cm^{-1}; and ferrocytochrome b_5, ν_4 = 1361 cm^{-1}; see Table III). Furthermore, the Soret maxima for P450 m^{rs} and m^r are found at ~408 nm, while the Soret band of P420 m^r is at 423 nm. Taken together, these spectroscopic observations suggest that, in the P420 m^r state, the thiolate ligand has been completely replaced by a more weakly electron-donating axial heme ligand. The further destabilization and loss of the thiolate ligand

[4] Well-defined optical spectra of pentacoordinate aquoligated ferric heme model complexes are not readily available and would be useful in helping to interpret the absorption spectra of low pH metMb (Sage et al., 1991a) as well as the spectra presented here. We cannot exclude the possibility that both water and thiolate (or histidine in the case of low pH metMb) are replaced by an unknown ligand; however, the retention of water as the fifth ligand is the simplest possibility, and we hold to this model until excluded by further experimental evidence. It should also be noted that the dissociation of the thiolate ligand is likely to be coupled with a protonation step.

Table III: Summary of Spectroscopic Data for Various Ferrous Heme Proteins[a]

heme protein	Soret max	β/α max	ν_4	ν_3	ν_2	ν_{FeHis}	spin	Fe^{II} ligation
P450 m^{rs}	408	544	1345	1466	1570		HS,5C	(Cys)S–Fe
ferrocytochrome c[b]	415	520/550	1361	1493	1592		LS,6C	His–Fe–S(Met)
ferrocytochrome b_5[c]	423	527/558	1361	1496	1586		LS,6C	His–Fe–His
P420 m^r	~423	530/558	1361	1493	1583		LS,6C	X–Fe–Y
				1470	1560		HS,5C	X–Fe
P420 M^{r*}	?	?	1354	1470	1561	220	HS,5C	His–Fe
deoxyMb pH 7	435	556	1357	1471	1563	220	HS,5C	His–Fe
deoxyMb, pH 2.6[d]	426	538/563	1356	1471	1562		HS,5C	H_2O–Fe

[a] All units for Raman modes are cm^{-1}, and for absorption bands, nm. [b] Remba et al. (1979). [c] Sligar et al. (1987). [d] Han et al. (1990).

upon reduction of P420 is consistent with the fact that the ferrous heme possesses a net neutral charge and is less likely to bind the negatively charged thiolate than the positively charged ferric heme.

The doublet structure observed in the ν_3 region (Figure 6) is evidence that ferrous P420 consists of a mixture of LS,6C and HS,5C states and again suggests a simple equilibrium for the ferrous heme ligation:

$$X\text{–}Fe^{2+}\text{–}Y \overset{K_3}{\rightleftharpoons} X\text{–}Fe^{2+} + Y \qquad (2)$$

The two ligation states involve a dissociable axial ligand (i.e., Y in eq 2) and account for the HS,5C species, with ν_3 = 1470 cm^{-1}, and the LS,6C species, with ν_3 = 1493 cm^{-1}. From the arguments above, we do not expect that either X or Y is a thiolate ligand.

A low pH deoxyMb species that spectroscopically resembles the HS,5C fraction of P420 m^r was recently observed by Han et al. (1990) using rapid mixing techniques. Han et al. (1990) noted the lack of a ν_{FeHis} mode in the Raman spectra of deoxyMb at pH 2.6 and attributed the other spectral features to a HS,5C ferrous state with H_2O as the most probable fifth ligand. As shown in Table III, the HS,5C ν_3 and ν_2 modes of P420 m^r have similar positions to those of deoxyMb at pH 2.6, and there is no evidence of a ν_{FeHis} mode in either complex. Both deoxyMb at pH 2.6 and P420 m^r possess doublet structures in the α/β band region, and their Soret bands are found at 426 and 423 nm, respectively. The similarities in the spectral features, and the lack of a ν_{FeHis} mode, suggests that the HS,5C population of P420 m^r possesses a weak-field (non-histidine) fifth ligand such as H_2O (X in eq 2).

Several residues are found near the heme site of $P450_{cam}$ and could become a heme ligand when the protein undergoes the tertiary structure change associated with P420 formation. These include the proximal His(355), proximal His(361), distal Tyr(96), and distal Thr(252) (Poulos et al., 1987). As discussed below, the 10-ns transient Raman spectrum of the photolyzed CO complex of P420 (m^{r*}) exhibits a band at ~218 cm^{-1} that is quite likely a ν_{FeHis} mode (Kitagawa, 1988). This strongly suggests that P420 m^r_{CO} possesses a histidine heme ligand and that the distinct photolyzed state m^{r*} evolves toward m^r on a time scale that is much slower than 10 ns. Although the Raman spectrum of P420 m^r does not have a ν_{FeHis} mode, the possibility that the LS,6C component possesses a dissociable histidine heme ligand (i.e., Y = His in eq 2) cannot be excluded. Other histidine-ligated ferrous LS,6C complexes [for example, cytochrome b_5 (Sligar et al., 1987) and MbCO (Wells et al., 1991)] do not exhibit a ν_{FeHis} mode. Thus, the prime candidates for heme ligation in eq 2 are X = H_2O and Y = histidine.

Ligation State of P420 m^r_{CO} and P420 m^{r*}. The Raman and absorption spectra of P420 m^r_{CO} and His-ligated MbCO below pH 4.0 are strikingly similar (see Figure 8a,b). For example, both exhibit Soret maxima at 423 nm, and the core size markers are all in nearly the same positions, ν_4 = 1372–1374, ν_3 = 1498–1501 cm^{-1}, and ν_2 = 1583–1584 cm^{-1}. In addition, the $\nu_{Fe\text{–}CO}$ positions are very similar, 491–494 cm^{-1}. The 30-cm^{-1} upshift of the $\nu_{Fe\text{–}CO}$ mode in the CO adduct of P420 from that of P450 m^r_{CO} is strong evidence for the loss of the thiolate heme ligand. The frequency of the Fe–CO mode is in the range expected for a His-ligated heme–CO complex such as the open pocket state of MbCO (Morikis et al., 1989). In general, the Raman spectral patterns of P420 m^r_{CO} and low pH MbCO are remarkably similar in all frequency regions. Moreover, the 10-ns transient photoproduct, P420 m^{r*}, possesses a distinct mode at 218 cm^{-1}, strongly indicating histidine ligation in the CO complex (see Figure 8d).

The Raman spectra of ferrous P420, discussed above, indicate the presence of a dissociable heme ligand, and we have suggested that Y = His in eq 2. The observation that P420 m^r_{CO} is histidine-ligated is consistent with this suggestion if, upon introduction of CO to P420 m^r, the water ligand (X) is displaced by CO. The binding of CO involves π back-donation from the iron to the CO and leads to a more acidic heme iron, having a higher affinity for the histidine ligand. The complete loss of the thiolate ligand is evidently due to tertiary structure rearrangements in P420 m^r that do not allow Cys357 access to the heme site.

As mentioned above, the Raman spectrum of P420 m^{r*} (see Figure 8) strongly indicates that it is a histidine-ligated HS,5C species due to the positions of ν_4 (1354 cm^{-1}), ν_3 (1470 cm^{-1}), ν_2 (1561 cm^{-1}), and the observation of a mode at 218 cm^{-1} (ν_{FeHis}). The positions of the ν_4, ν_3, and ν_2 modes in the HS,5C state of P420 m^{r*} are similar to those of P420 m^r (see Table III), but P420 m^r lacks the 218-cm^{-1} band. These observations suggest that the 10-ns Raman spectrum probes a histidine-ligated transient state distinct from the equilibrium HS,5C population of P420 m^r, which possesses a weak-field fifth ligand, possibly H_2O.

Substrate Equilibrium and Photolysis of P450 and P420 m^{rs}_{CO}. As discussed under Results, two $\nu_{Fe\text{–}CO}$ modes are observed in the Raman spectrum of P450 m^{rs}_{CO} when the sample cell is static. These modes correspond to the camphor-bound and camphor-free P450 CO complexes (Uno et al., 1985). Thus, photolysis of the CO ligand in P450 m^{rs}_{CO} induces dissociation of the camphor substrate from the heme pocket. Similar conclusions have been drawn from photoacoustic calorimetry experiments where photolysis of CO leads to a time-dependent heat function in the nanosecond regime, which is believed to be due to camphor leaving the pocket (S. Sligar, G. Hui Bon Hoa, C. Di Primo, unpublished results).

The above observations strongly suggest that some fraction of the total translational and rotational kinetic energy (~5–10 kcal/mol) of the photolyzed CO molecule is transferred to the camphor substrate, causing its dissociation from the protein-binding site. Since catalytic efficiency demands that there be a close proximity between the bound diatomic molecule and

Table IV: ν_{Fe-CO} Bands at P450 with Various Substrates[a]

sample	substrate	ν_{Fe-CO}
P450	absent	465
P450	TMCH[b,d]	485
P450	Fenchone[d]	480
P450	CPRQ[c,d]	476
P450	camphor	484
P420	absent	496
P420	camphor	494

[a] All units are cm^{-1}. [b] Tetramethylcyclohexanone. [c] Camphoroquione. [d] Data for TMCH, Fenchone and CPRQ from Bangcharoenpaurpong (1987).

the substrate, it is not surprising that an exchange of kinetic energy takes place between the photolyzed CO and the camphor substrate.

Further evidence that the CO ligand and substrate interact is given in Table IV, which reports the ν_{Fe-CO} frequencies when several different organic substrates are bound to P450 (Uno et al., 1985; Bangcharoenpaurpong, 1987). It is apparent that the ν_{Fe-CO} mode of P450 is highly sensitive to substrate, indicating a direct interaction between the bound CO and the substrate molecule. This is also consistent with the IR absorption work of O'Keeffe et al. (1978) and Jung and Marlow (1987), which found that the ν_{CO} frequency for the CO complex of P450 was highly sensitive to camphor binding. Camphor-bound P450 m^{rs}_{CO} has ν_{CO} ~1940 cm^{-1}, and camphor-free P450 m^{r}_{CO} has at least two bands at ~1942 and 1963 cm^{-1}. O'Keeffe et al. assigned the ~1940-cm^{-1} bands to a bent geometry and the ~1960-cm^{-1} band to an upright geometry for the Fe–C–O moiety. Similar assignments have also been made for the bent and upright conformers of MbCO (Shimada & Caughey, 1982; Morikis et al., 1989; Ansari et al., 1987).

We have also observed that the ν_{Fe-CO} mode of substrate-free P450 m^{r}_{CO} (at 465 cm^{-1}) increases intensity with respect to the ν_{Fe-CO} mode for substrate-bound P450 (at 484 cm^{-1}) as the incident laser power is increased in the static cell experiment. This indicates that CO reacts more rapidly with the camphor-free protein and rebinds before the camphor can re-enter the heme pocket. This observation is qualitatively consistent with the measured rebinding rate for CO in the presence and absence of camphor, which is two orders of magnitude faster in camphor-free than in camphor-bound P450 (Peterson & Griffin, 1972).

In contrast to P450, the Raman spectrum of the CO complex of P420 is insensitive to substrate and has only one mode in the ν_{Fe-CO} region. This suggests that camphor is unable to bind in close proximity to the Fe–CO moiety in P420. Evidently, the tertiary changes associated with P420 formation alter the protein conformation so that histidine ligation is favored in the CO complex, and the distal pocket is modified so that substrate binding is minimized or located farther away from the distal heme site. This latter suggestion is in accord with the work of O'Keeffe et al. (1978), who found the ν_{CO} mode of CO-bound P420 at 1966 cm^{-1} in the presence of camphor. This indicates that the FeCO moiety of P420 has upright geometry and supports the conclusion that the camphor-binding pocket is somehow altered so that substrate does not interact directly with the CO ligand. It should be noted, however, that camphor binding to P420 does lead to decreased CO photolysis yields.

SUMMARY

In summary, we have found that cytochrome P420, the inactive form of cytochrome P450, does not bind camphor in a way that significantly alters the heme ligation state or heme environment in the ferric, ferrous, or ferrous CO-bound states. The appearance of two core size ν_3 modes in the oxidized and reduced forms of P420 indicates that the heme of ferric and ferrous P420 is involved in equilibria between spin/coordination states (see eqs 1 and 2).

Ferric P420 consists of a LS,6C heme ligation state that spectroscopically resembles P450 m^{o} [with Cys(357) and H_2O as axial heme ligands] in equilibrium with a HS,5C heme where the thiolate-iron bond is broken and the H_2O remains as the likely fifth ligand. The Cys(357) bond is evidently destabilized in ferric P420 by tertiary conformational alterations of the protein that lead to changes in the equilibrium constant K_1 in eq 1. The HS,5C form is spectroscopically similar to metMb below pH 4.0, which lacks the proximal histidine ligand and is thought to have H_2O as the fifth ligand.

Ferrous P420 is also in equilibrium between LS,6C and HS,5C heme ligation states. Since ferrous P420 lacks the downshifted ν_4 band, thiolate ligation is unlikely in the ferrous state. Spectral comparisons with a low pH form of deoxyMb suggests that H_2O is a good candidate for the heme ligand in the 5C,HS state. The fact that histidine ligation is observed in the CO adduct of P420 suggests that it may be the (dissociable) ligand in the 6C,LS state of ferrous P420 (i.e., Y in eq 2).

The heme–CO complex of P420 involves histidine ligation, on the basis of the appearance of a 218-cm^{-1} mode in the 10-ns transient, and the P420 m^{r}_{CO} Raman and absorption spectra, which strongly resemble those of low pH MbCO, a species which is known to have a histidine heme ligand (Sage et al., 1991a). The position of the ν_4 mode of P420 m^{r*} differs significantly from that of equilibrium P420 m^{r}, which, in addition to the appearance of the 218-cm^{-1} mode, indicates that the P420 m^{r*} spectrum probes a transient state which is distinct from the equilibrium P420 m^{r} state. This behavior is analogous to that found for the low pH form of Mb (Sage et al., 1991a,b) and is quite likely due to the acidification of the heme iron atom in the CO-bound complex, which increases the affinity for histidine ligation to the heme.

We have also found that substrate dissociation can be induced by CO photolysis in P450 m^{rs}_{CO}, indicating that camphor and CO can efficiently exchange kinetic energy. The photolysis data are consistent with substrate binding that is slow compared to the CO binding rates and with enhanced CO binding when substrate is not in the heme pocket.

Overall, the evidence indicates that the heme environment and the camphor-binding site of P420 differ sharply from that of P450. This is probably due to an altered tertiary protein structure that leads to changes in key equilibrium constants associated with heme ligation and substrate binding.

Registry No. Cytochrome P450, 9035-51-2; cytochrome P420, 9035-49-8.

REFERENCES

Abe, M., Kitagawa, T., & Kyogoka, Y. (1978) *J. Chem. Phys. 69*, 4526.

Andersson, L. A., Mylrajan, M., Sullivan, E., & Strauss, S. (1989) *J. Biol. Chem. 32*, 19099.

Ansari, A., Berendzen, J., Braunstein, D., Cowen, B. R., Fraunfelder, H., Hong, M. K., Iben, I. E. T., Johnson, J. B., Ormos, P., Sauke, T. B., Scholl, R., Schulte, A., Steinbach, P. J., Vittitow, J., & Young, R. D. (1987) *Biophys. Chem. 26*, 337.

Anzenbacher, P., Evangelista-Kirkup, R., Schenkman, J., & Spiro, T. G. (1989) *Inorg. Chem. 28*, 4491.

Bangcharoenpaurpong, O. (1987) Ph.D. Thesis, Northeastern University, Boston, MA.

Bangcharoenpaurpong, O., Rizos, A. K., Champion, P. M., Jollie, D., & Sligar, S. G. (1986) *J. Biol. Chem. 261*, 8089.
Bangcharoenpaurpong, O., Champion, P. M., Martinis, S. A., & Sligar, S. G. (1987) *J. Chem. Phys. 87*, 4273.
Caughey, W. S., Alben, J. O., McCoy, S., Boyer, S. H., Charache, S., & Hathaway, P. (1969) *Biochemistry 8*, 59.
Champion, P. M. (1988) in *Biological Applications of Raman Spectroscopy* (Spiro, T. G., Ed.) Vol. 3, p 249, John Wiley & Sons, New York.
Champion, P. M. (1989) *J. Am. Chem. Soc. 111*, 3433.
Champion, P. M., Gunsalus, I. C., & Wagner, G. C. (1978) *J. Am. Chem. Soc. 100*, 3743.
Champion, P. M., Stallard, B. R., Wagner, G. C., & Gunsalus, I. C. (1982) *J. Am. Chem. Soc. 104*, 5469.
Choi, S., & Spiro, T. G. (1983) *J. Am. Chem. Soc. 105*, 3683.
Choi, S., Spiro, T. G., Langry, K. C., Smith, K. M., Budd, D., & La Mar, G. (1982) *J. Am. Chem. Soc. 104*, 4345.
Chottard, G., Schappacher, M., Ricard, L., & Weiss, R. (1984) *Inorg. Chem. 23*, 4557.
Dawson, J. H. (1988) *Science 240*, 433.
Dawson, J. H., & Sono, M. (1987) *Chem. Rev. 87*, 1255.
Debrunner, P. G., Gunsalus, I. C., Sligar, S. G., & Wagner, G. C. (1978) in *Metal Ions in Biological Systems* (Siegal, H., Ed.) Vol. 7, p 241, Marcel Dekker, New York.
Egawa, T., Ogura, T., Makino, R., Ishimura, Y., & Kitagawa, T. (1991) *J. Biol. Chem. 266*, 10246.
Fisher, M., & Sligar, S. G. (1987) *Biochemistry 26*, 4797.
Griffin, B. A., & Peterson, J. A. (1972) *Biochemistry 11*, 4740.
Groves, J., Haushalter, R., Nakamura, M., Nemo, T., & Evans, B. (1981) *J. Am. Chem. Soc. 103*, 2884.
Guengerich, F. P. (1991) *J. Biol. Chem. 266*, 10019.
Gunsalus, I. C., Meeks, J. R., Lipscomb, J. D., Debrunner, P., & Munck, E. (1974) in *Molecular Mechanisms of Oxygen Activation* (Hayishi, O., Ed.) p 559, Academic Press, New York.
Han, N., Rousseau, D. L., Giacometti, G., & Brunori, M. (1990) *Proc. Natl. Acad. Sci. U.S.A. 87*, 205.
Hanson, L. K., Eaton, W. A., Sligar, S. G., Gunsalus, I. C., Gouterman, M., & Connell, C. R. (1976) *J. Am. Chem. Soc. 98*, 2672.
Hildebrandt, P., Greinert, R., Stier, A., & Taniguchi, H. (1989) *Eur. J. Biochem. 186*, 291.
Hu, S., & Kincaid, J. R. (1991) *J. Am. Chem. Soc. 113*, 2843.
Hu, S., Schneider, A. J., & Kincaid, J. R. (1991) *J. Am. Chem. Soc. 113*, 4815.
Koga, H., Rauchfuss, B., & Gunsalus, I. C. (1985) *Biochem. Biophys. Res. Commun. 130*, 412.
Hui Bon Hoa, G., Di Primo, C., Dondaine, I., Sligar, S. G., Gunsalus, I. C., & Douzou, P. (1989) *Biochemistry 28*, 651.
Jung, C., & Marlow, F. (1987) *Stud. Biophys. 120*, 241.
Kitagawa, T. (1988) in *Biological Applications of Raman Spectroscopy* (Spiro, T. G., Ed.) Vol. 3, p 97, John Wiley & Sons, New York.
Li, X. Y., Czernuszewicz, R. S., Kincaid, J. R., & Spiro, T. G. (1989) *J. Am. Chem. Soc. 111*, 7012.
Li, X. Y., Czernuszewicz, R. S., Kincaid, J. R., Su, Y. O., & Spiro, T. G. (1990a) *J. Phys. Chem. 94*, 31.
Li, X. Y., Czernuszewicz, R. S., Kincaid, J. R., Stein, P., & Spiro, T. G. (1990b) *J. Phys. Chem. 94*, 47.
Lipscomb, J. D. (1980) *Biochemistry 19*, 3590.
Martinis, S. A. (1990) Ph.D. Thesis, Department of Biochemistry, University of Illinois, Urbana-Champaign, IL.
Morikis, D. (1990) Ph.D. Thesis, Department of Physics, Northeastern University, Boston, MA.
Morikis, D., Champion, P. M., Springer, B. A., & Sligar, S. G. (1989) *Biochemistry 28*, 4791.
Morikis, D., Li, P., Bangcharoenparpong, O., Sage, J. T., & Champion, P. M. (1991) *J. Phys. Chem. 95*, 3391.
O'Keeffe, D. H., Ebel, R. E., Peterson, J. A., Maxwell, J. C., & Caughey, W. S. (1978) *Biochemistry 17*, 5845.
Ozaki, Y., Kitagawa, T., Kyogoku, Y., Imai, Y., Hashimoto-Yutsudo, C., & Sato, R. (1978) *Biochemistry 17*, 5826.
Peterson, J. A., & Griffin, B. A. (1972) *Arch. Biochem. Biophys. 151*, 427.
Poulos, T. L., Finzel, B. C., & Howard, A. J. (1986) *Biochemistry 25*, 5314.
Poulos, T. L., Finzel, B. C., & Howard, A. J. (1987) *J. Mol. Biol. 195*, 687.
Raag, R., & Poulos, T. L. (1989a) *Biochemistry 28*, 917.
Raag, R., & Poulos, T. L. (1989b) *Biochemistry 28*, 7586.
Remba, R. D., Champion, P. M., Fitchen, D. B., Chiang, R., & Hager, L. P. (1979) *Biochemistry 18*, 2280.
Sage, J. T., Morikis, D., & Champion, P. M. (1991a) *Biochemistry 30*, 1227.
Sage, J. T., Li, P., & Champion, P. M. (1991b) *Biochemistry 30*, 1237.
Shimada, H., & Caughey, W. S. (1982) *J. Biol. Chem. 257*, 11893.
Sligar, S. G. (1976) *Biochemistry 15*, 5399.
Sligar, S. G., & Gunsalus, I. C. (1976) *Proc. Natl. Acad. Sci. U.S.A. 73*, 1078.
Sligar, S. G., Egeberg, K. D., Sage, J. T., Morikis, D., & Champion, P. M. (1987) *J. Am. Chem. Soc. 109*, 7896.
Spaulding, L., Chang, C., Yu, N. T., & Felton, R. (1975) *J. Am. Chem. Soc. 97*, 2517.
Spiro, T. G. (1983) in *Iron Porphyrins* (Lever, A. B. P., & Gray, H. B., Eds.) Part II, p 91, Addison-Wesley, New York.
Tsubaki, M., Hiwatashi, A., & Ichikawa, Y. (1987) *Biochemistry 26*, 4535.
Unger, B. P., Gunsalus, I. C., & Sligar, S. G. (1986) *J. Biol. Chem. 261*, 1158.
Uno, T., Nishimura, Y., Makino, R., Iizuka, T., Ishimura, Y., & Tsuboi, M. (1985) *J. Biol. Chem. 260*, 2023.
Wells, A. V., Sage, J. T., Morikis, D., Champion, P. M., Chiu, M. L., & Sligar, S. G. (1991) *J. Am. Chem. Soc. 113*, 9655.